Immunity, Vol. 18, 343–354, March, 2003, Copyright ©2003 by Cell Press

Quantitating Protein Synthesis, Degradation, and Endogenous Antigen Processing

Michael F. Princiotta,[1] Diana Finzi,[1] Shu-Bing Qian,[1] James Gibbs,[1] Sebastian Schuchmann,[2] Frank Buttgereit,[2] Jack R. Bennink,[1] and Jonathan W. Yewdell[1,*]

[1]Laboratory of Viral Diseases
National Institute of Allergy and Infectious Diseases
Bethesda, Maryland 20892

[2]Department of Rheumatology and Clinical Immunology
Charité University Hospital
Humboldt University
10117 Berlin
Germany

Summary

Using L929 cells, we quantitated the macroeconomics of protein synthesis and degradation and the microeconomics of producing MHC class I associated peptides from viral translation products. To maintain a content of 2.6 × 10^9 proteins, each cell's 6 × 10^6 ribosomes produce 4 × 10^6 proteins min^{-1}. Each of the cell's 8 × 10^5 proteasomes degrades 2.5 substrates min^{-1}, creating one MHC class I-peptide complex for each 500–3000 viral translation products degraded. The efficiency of complex formation is similar in dendritic cells and macrophages, which play a critical role in activating T cells in vivo. Proteasomes create antigenic peptides at different efficiencies from two distinct substrate pools: rapidly degraded newly synthesized proteins that clearly represent defective ribosomal products (DRiPs) and a less rapidly degraded pool in which DRiPs may also predominate.

Introduction

Contemporary cell biology is dominated by reductionist approaches. Faced with the daunting complexity of cells, cell and molecular biologists typically examine isolated components of systems without accounting for their place in the larger scheme. Despite the fact that quantitative aspects of systems are critical to their understanding, they are frequently ignored.

A case in point is protein synthesis and degradation, clearly two of the more important tasks performed by cells. There has been remarkable progress toward understanding how proteins are degraded by eukaryotic cells (Hershko and Ciechanover, 1998; Rock and Goldberg, 1999). Scant attention has been paid, however, to quantitative aspects of degradation. Clearly, protein synthesis and degradation must be balanced for cells to maintain viability. The degradative machinery must have sufficient baseline capacity to dispose of damaged or defective proteins produced by cells under normal conditions and sufficient excess capacity to cope with various forms of physical or chemical stress that rapidly increase protein turnover. Cell growth or activation is also expected to increase the protein disposal rate due to increased rates of protein synthesis and also the redistribution of cellular resources to new tasks.

Extending the previous work of Wheatley (1989), we recently provided evidence that a significant fraction (upwards of 30%) of proteins are degraded by proteasomes shortly after their synthesis, presumably due in large part to their inability to achieve a functional state (we have termed such proteins defective ribosomal products [DRiPs]) (Schubert et al., 2000). One explanation for the apparent inefficiency in protein synthesis is that it is less costly for cells to degrade a high fraction of defective proteins than it is to synthesize proteins more efficiently. To evaluate the costs, we need to know the rate of protein synthesis and its energetic costs. We also need to know the number of proteasomes and the turnover rates required for degradation of such a large fraction of nascent proteins.

The importance of understanding protein degradation in quantitative terms is heightened by its contribution to immune surveillance. The vertebrate immune system uses the peptide products of proteasomal degradation to monitor the presence of viruses and other intracellular parasites (Rock et al., 2002). A fraction of proteasomal peptides find their way to class I molecules of the major histocompatibility complex (MHC) which display them on the cell surface for perusal by T cell receptors on $CD8^+$ T cells (T_{CD8+}).

Many quantitative aspects of antigen processing are uncertain. What fraction of viral peptides derives from DRiPs? What is the efficiency of generating peptides from proteasomal substrates? Do these numbers vary widely between different substrates? What are the rates of peptide generation and class I transport? What is the capacity of the class I presentation system?

In this study we provide answers to these questions, show that the rate of class I peptide complex formation can be used to estimate the rate of DRiP formation (referred to henceforth as the "DRiP rate") of a given substrate, and relate the economics of antigen processing to the overall protein and energy economies of the cell.

Results

The Protein Economy of L-K^b Cells

In the studies that follow we primarily use mouse L929 cells. To employ the 25-D1.16 mAb for quantitating peptide class I complexes (Porgador et al., 1997), we used cells transfected with a cDNA encoding the mouse H-2 K^b class I molecule (termed L-K^b cells).

Our first (and easiest) step in characterizing the protein economy of L-K^b cells was to determine their protein content. This amounted to 200 pg $cell^{-1}$ as determined by the Biorad DC protein assay or 2.6 × 10^9 copies $cell^{-1}$ of a typical protein defined as consisting of 466 amino acid residues (the average length in the EMBL human

*Correspondence: jyewdell@nih.gov

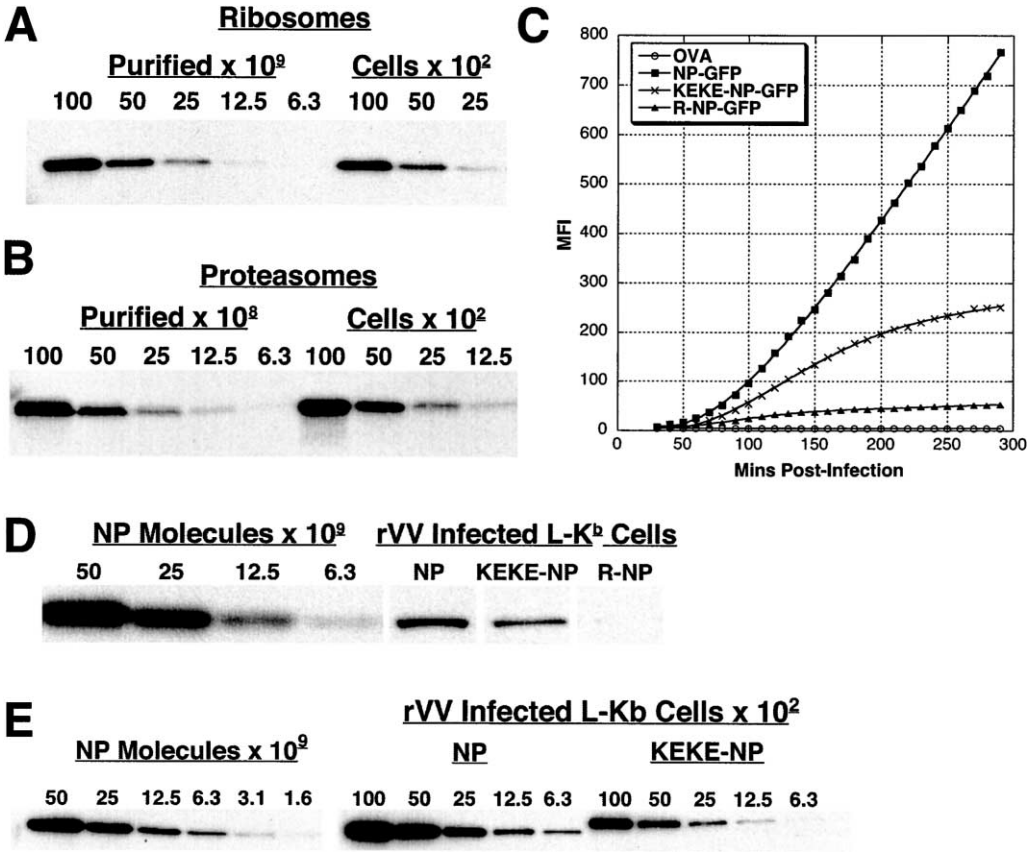

Figure 1. Determination of Protein Concentrations in L-K^b Cells

(A and B) Two-fold serial dilutions of lysates from L-K^b cells infected with rVV-expressing NP-GFP or uninfected control cells were immunoblotted for ribosomes (A) or proteasomes (B). Purified ribosome and proteasome preparations were used to generate standard curves to determine proteasome and ribosome concentrations.

(C) Accumulation of chimeric NP-GFP molecules in L-K^b cells infected with rVV-expressing NP-GFP (squares), KEKE-NP-GFP (X), R-NP-GFP (triangles), or OVA (circles). Note that nonfluorescent OVA defines autofluorescence levels.

(D) (Right side) L-K^b cells (10^4 cells/lane) infected with rVV-expressing chimeric NP-GFP 2.5 hr p.i. and immunoblotted with NP-specific antibodies. (Left side) Purified influenza nucleoprotein added to uninfected cell lysates was run on the same gel to generate a standard curve.

(E) (Right side) L-K^b cells (cell number per lane indicated) infected with rVV-expressing NP-GFP or KEKE-NP-GFP 5 hr p.i. and immunoblotted with anti-NP antibodies. Uninfected cell lysates were added to samples to maintain 10^4 cell equivalents per lane. (Left side) Same as for (D).

proteome). Next, we used quantitative Western blotting in conjunction with purified ribosome and proteasome standards to determine copy numbers. L-K^b cells possess 6×10^6 ribosomes and 10^6 proteasomes cell^{-1} (Figures 1A and 1B). We need to correct these figures to account for subunits that are not present in functional assemblies. For ribosomes, this should be minimal since the half-life of assembled ribosomes (10 d) is much longer than their assembly time (Nissen-Meyer and Eikhom, 1976). There is no comparable data for proteasomes in L929 cells, but it has been reported that 75%–80% of proteasome subunits are present in functional assemblies in a rapidly dividing mouse cell line (Nandi et al., 1997). Extrapolating this result to L-K^b cells results in a copy number of $\sim 8 \times 10^5$ functional proteasomes cell^{-1}.

We next measured the rate of protein synthesis by measuring the incorporation of ^{3}H-Leu into TCA insoluble material by L-K^b cells labeled in normal growth media (see Experimental Procedures). The apparent rate of protein synthesis was 3.3×10^6 proteins min^{-1}. This does not account for DRiPs, however, some of which are degraded during pulse labeling (Schubert et al., 2000). To estimate the fraction of newly synthesized proteins degraded under these conditions, we radiolabeled cells in the presence and absence of proteasome inhibitors. These data indicate that the true rate of protein synthesis is $\sim$25% greater than the measured rate in the absence of proteasome inhibitors, or $\sim 4 \times 10^6$ proteins min^{-1}. This value is consistent with the ribosome count; given a typical translation rate of 5 amino acid residues s^{-1} (Palmiter, 1975), each ribosome can produce a typical protein every 93 s, which amounts to 3.9×10^6 proteins cell^{-1} min^{-1} if all ribosomes are translating proteins at this rate. Our data indicate that there are few idle ribosomes in L-K^b cells.

Can we account for the fate of the 4×10^6 proteins produced each min? Based on recovery of TCA insoluble material in pulse-chase experiments, we find that 1.3×10^6 proteins min^{-1} are degraded by proteasomes within the first 2 hr of their synthesis (1×10^6 min^{-1} in the first 10 min), 4.7×10^5 proteins min^{-1} are secreted

Table 1. Chimeric Protein Construct Names and Descriptions

Name	Protein	Description
NP-GFP	NP-SIINFEKL-EGFP	Stable, nuclear form of protein
R-NP-GFP	Ub-R-NP-SIINFEKL-EGFP	Posttranslationally degraded ($t_{1/2} \sim 10$ min)
KEKE-NP-GFP	NP-KEKE-SIINFEKL-EGFP	Misfolded NP; forms an unstable cellular pool of protein ($t_{1/2} \sim 70$ min)
OVA	Chicken egg ovalbumin	Full-length ovalbumin; secreted protein; no cellular protein pool accumulates
MSIINFEKL	SIINFEKL peptide	Minimal K^b binding peptide with amino terminal met from initiating AUG

or released from cells within an hour of their synthesis, and a further 5×10^5 proteins min^{-1} are degraded over the next 22 hr based on a measured turnover rate of 1.1% of long-lived proteins per hour (see Experimental Procedures). This would leave 1.7×10^6 proteins min^{-1} to create a daughter L-K^b cell, which is remarkably close to the number of proteins (1.8×10^6 min^{-1}) needed to double cellular protein content to support a cell division time of 24 hr.

We next determined the energetic cost of protein synthesis in L-K^b cells. When protein synthesis was blocked by adding cycloheximide to cells, oxygen consumption was reduced by 34%. We measured the efficiency of producing ATP from O_2 under these conditions to be 75% (using oligomycin to block the mitochondrial ATPase), meaning that protein synthesis consumes ~45% of cellular ATP supplies. This is a minimal estimate of the cellular energy that is devoted to protein synthesis since, using the medium required for measuring ATP consumption, protein synthesis was diminished relative to cells incubated in growth medium. This underscores the high price that cells pay for protein synthesis, ~5 ATP per peptide bond or 2300 ATP per typical protein. The cost of DRiPs in energetic terms is correspondingly high: a DRiP rate of 25% corresponds to ~11% of total cellular energy usage.

In addition, we found that treating L-K^b cells with the proteasome inhibitor lactacystin did not result in any detectable reduction in oxygen consumption (data not shown). Although proteasome mediated protein degradation consumes ATP, the amount of ATP used would have to be on the order of 150 ATPs $substrate^{-1}$ to account for even a 1% reduction in oxygen consumption, given a proteasome-mediated degradation rate of 1.8×10^6 proteins min^{-1}. A 1% reduction in oxygen consumption is below the sensitivity of detection of the method used. Even if proteasome ATP consumption is larger than this, it might not be inhibited by proteasome inhibitors, since the energy is expended by the 19S subunit which may continue to function while attached to inactivated 20S proteasomes.

Quantitating Antigen Processing in L-K^b Cells

Step 1: Quantitating Substrate Synthesis

Several recent studies suggest that a large portion of the peptides presented by MHC class I molecules on the cell surface are derived from nascent proteins (Schubert et al., 2000; Reits et al., 2000; Khan et al., 2001). To gain a more quantitative understanding of peptide generation, we used a panel of recombinant vaccinia viruses (rVV) that express chimeric proteins containing influenza nucleoprotein (NP), a 498 residue protein with an extremely high metabolic stability as measured by standard means (Table 1).

The first construct expresses NH_2-terminal NP fused with the chicken egg ovalbumin-derived K^b binding SIINFEKL peptide and enhanced green fluorescence protein (GFP) at the COOH terminus (this chimera is termed NP-GFP). In the second chimera, a sequence consisting largely of repeated Lys-Glu residues is inserted into NP-GFP (KEKE-NP-GFP) (Antón et al., 1999). The KEKE motif causes NP-GFP to misfold and is degraded by the ubiquitin (Ub)-proteasome system with a $t_{1/2}$ of ~70 min in L-K^b cells (data not shown). In the third chimera, the initiating Met of NP-GFP is replaced by Arg fused at the COOH terminus of Ub (R-NP-GFP). Ub is cotranslationally cleaved by Ub hydrolases, and the remaining protein is degraded by proteasomes with a $t_{1/2}$ of 10 min in L-K^b cells (data not shown).

Following infection of L-K^b cells with rVVs, GFP synthesis was monitored by flow cytometry at 10 min intervals for 5 hr. Between 50 and 60 min after adding VV-NP-GFP to cells, we first detected GFP, whose rate of accumulation accelerated until peaking approximately 30 min later (Figure 1C). Detection of the modified NP-GFP chimeras displayed similar kinetics, but with a gentler slope that eventually decelerated as the rate of degradation matched the rate of synthesis. The character of these curves is completely consistent with the measured biochemical half-lives of the respective proteins (Figure 1D).

We measured the amount of NP-GFP fusion proteins by quantitative Western blotting (Figure 1E). This revealed that 1 fluorescent unit corresponds to 1×10^4 molecules, and therefore the cellular concentration of NP-GFP 5 hr after infection is 8×10^6 molecules $cell^{-1}$. Starting at ~90 min postinfection, NP-GFP accumulates at a rate of 2.2×10^6 molecules hr^{-1}.

We confirmed the validity of these figures by metabolic radiolabeling. VV-NP-GFP infected cells were radiolabeled with [^{35}S]-Met. After resolving [^{35}S]-Met labeled proteins via SDS-PAGE, we used a PhosphorImager to determine the fraction of radioactivity incorporated in NP-GFP. Taking into account the Met content of NP-S-GFP, we calculated that NP-GFP production ranged from 1.4% to 2.5% of the total protein synthesis in rVV-infected L-K^b cells in several different experiments. Based on the overall rate of protein synthesis determined using [^{3}H]-Leu to label a different aliquot of cells in the same experiment, we calculated that cells produced between $2.1–3.8 \times 10^6$ NP-GFP molecules hr^{-1}, which agrees with the Western blot data.

Radiolabeling further revealed that the rate of NP-GFP synthesis attained maximal levels approximately 30 min earlier than fluorescence as determined by flow cytometry. The acquisition of fluorescence by GFP expressed in bacteria under anaerobic conditions upon exposure to oxygen demonstrates similar kinetics ($t_{1/2} = 27$ min) (Heim et al., 1995), suggesting that the rate-limiting step

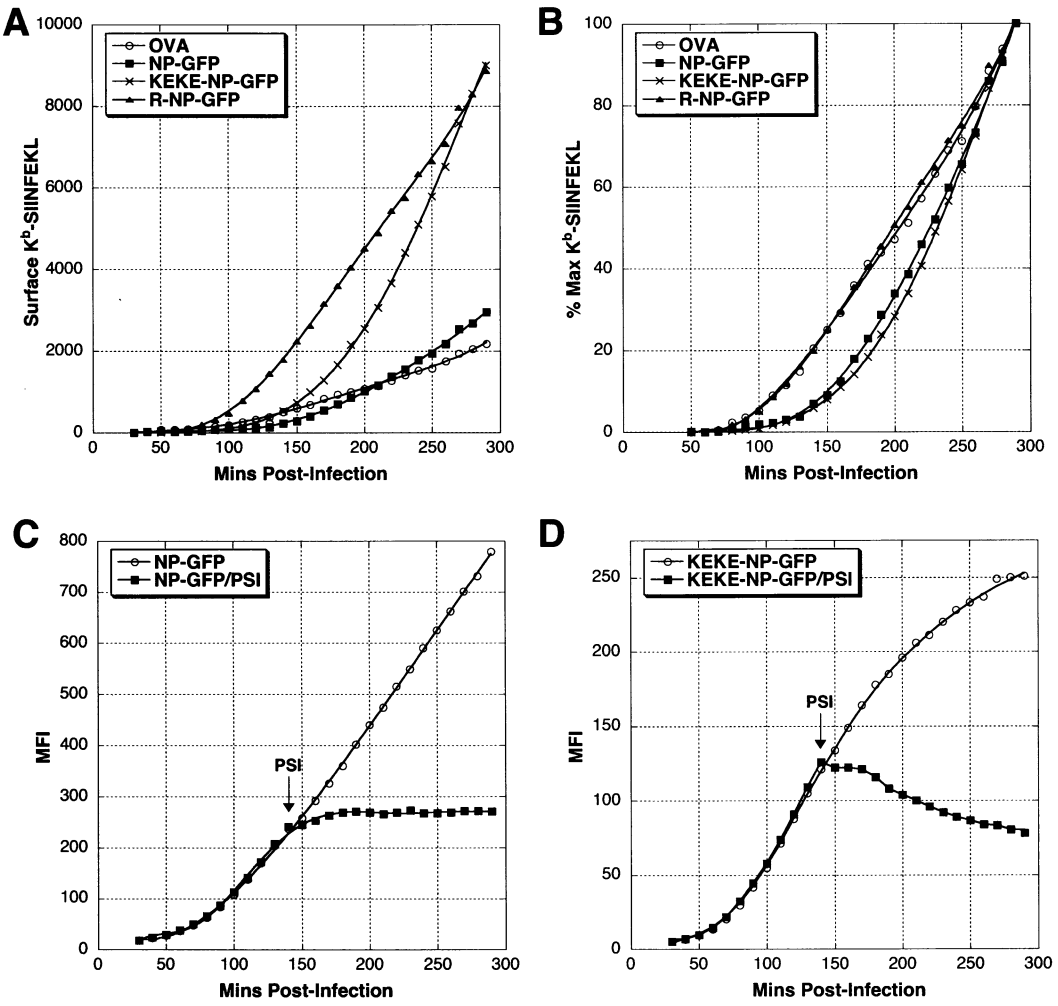

Figure 2. K^b-SIINFEKL and Chimeric NP-GFP Levels in rVV-Infected L-K^b Cells

(A) L-K^b cells were infected with rVVs expressing NP-GFP (squares), KEKE-NP-GFP (X), R-NP-GFP (triangles), or OVA (circles). Surface K^b-SIINFEKL complexes were quantitated by direct staining with Alexa Fluor 647-conjugated 25-D1.16 mAb.

(B) Surface K^b-SIINFEKL levels from (A) expressed as the percent of maximum expression for each construct. Graph symbols are the same as for (A).

(C and D) GFP levels in L-K^b cells infected with rVV-expressing NP-GFP (C) or KEKE-NP-GFP (D) and treated 140 min p.i. with protein synthesis inhibitors (squares) or left untreated (circles).

in GFP maturation in eukaryotic cells is also oxidation of the fluorophore.

Step 2: Quantitating Peptide Class I Complexes

We quantitated K^b-SIINFEKL complexes (hereafter referred to as complexes) using 25-D1.16 mAb conjugated to Alexa Fluor 647. By relating fluorescence intensity to a standard curve, we could determine the number of complexes present on the surface of rVV-infected cells shown in Figure 1C. In addition to the rVVs described above, we used rVVs encoding chicken egg ovalbumin (OVA) (the source of SIINFEKL) or MSIINFEKL.

As seen in Figure 2A, $\sim 3 \times 10^3$ complexes are generated after a 5 hr infection with either VV-NP-GFP or VV-OVA. Although R-NP-GFP is degraded rapidly, the number of complexes increases only 3-fold. By 5 hr postinfection a similar number of complexes are produced from KEKE-NP-GFP as from R-NP-GFP. Interestingly, the kinetics of peptide-class I complex generation markedly differs between these two substrates. While the rate of complex formation from R-NP-GFP plateaus at $\sim$110 min postinfection, the rate of complex formation from KEKE-NP-GFP accelerates throughout the infection period. This suggests that complexes are derived from two pools of KEKE-NP-GFP, one that is degraded rapidly and the other more slowly. As the latter pool accumulates, the absolute rate of degradation increases, and the rate of complex generation increases in step.

Note that the peptide generation curves for R-NP-GFP and KEKE-NP-GFP eventually cross. Since the rates of synthesis of the two proteins are similar (if anything, slightly more R-NP-GFP is synthesized) (data not shown), this indicates that the efficiency of generating SIINFEKL from the two proteins differs. Calculation of the slopes reveals that by 4 hr postinfection (p.i.), SIINFEKL is generated at twice the efficiency from KEKE-NP-GFP than from R-NP-GFP. This cannot be attributed to differences in local flanking sequences, since the proteins differ only

by the Ub extension (which is removed immediately) and the insertion of the KEKE sequence 165 residues upstream from SIINFEKL.

In Figure 2B, K^b-SIINFEKL levels are replotted as a percentage of the maximum surface levels at the end of the infection, revealing that the kinetics of K^b-SIINFEKL production from OVA and R-NP-GFP are remarkably similar. Following a lag period of 90 min p.i., rates rapidly reach maximal levels in parallel. This strongly suggests that nearly all peptides from OVA derive from DRiPs. By contrast, the relative rate of complex formation from NP-GFP is highly similar to KEKE-NP-GFP. This suggests that, as with KEKE-NP-GFP, peptides are derived from rapidly and slowly degraded forms of NP-GFP, with the latter being the more efficient source.

Contribution of Newly Synthesized Proteins to Antigen Processing

We further examined the contribution of nascent proteins to complex formation by treating cells with protein synthesis inhibitors (PSI) 140 min after the start of infection. Protein synthesis halted within a minute of adding PSI to cells, as determined by cessation of incorporation of [^{35}S]-Met. There was an immediate retardation in the rate of GFP accumulation. GFP continued, however, to accumulate at a lower rate for 40 min. This is consistent with the lag between radiolabeling and fluorescence noted above.

Importantly, the level of NP-GFP fluorescence remained essentially unchanged for the remainder of the 2.5 hr incubation period (Figure 2C). By contrast, the addition of PSI resulted in an immediate leveling off of KEKE-NP-GFP fluorescence for ~30 min, which then declined with a $t_{1/2}$ of 180 min (Figure 2D). We interpret the plateau to indicate a balance between the acquisition of fluorescence by nascent GFP and degradation. Notably, the fluorescent $t_{1/2}$ is considerably longer than the measured biochemical $t_{1/2}$ of KEKE-NP-GFP (~70 min). This indicates that there is heterogeneity of KEKE-NP-GFP with regard to fluorescence and, further, that fluorescence is associated with greater metabolic stability.

We examined complex formation in the same experiment. In cells expressing R-NP-GFP, addition of PSI did not affect complex generation for 50 min, when it abruptly ceased (Figure 3A). Since peptides are generated rapidly from this substrate, this demonstrates that 50 min are required for peptide processing, complex formation, and transporting complexes to the cell surface. This is in close agreement with the lag between the times required to achieve the maximal synthetic rate of VV-encoded proteins (90–100 min) and the maximal rate of peptide generation from R-NP-GFP (140–150 min). OVA behaved identically to R-NP-GFP (Figure 3B), demonstrating that, for this protein, peptides are derived nearly exclusively from a newly synthesized pool.

The production of complexes from NP-GFP and KEKE-NP-GFP demonstrated a different behavior. Like R-NP-GFP and OVA, both demonstrated the 50 min lag in which complex formation continued identically to untreated cells. However, rather than stopping at this time, complexes accumulated at a reduced rate for the next 90 min (Figures 3C and 3D). This demonstrates that the abrupt abrogation of complex formation from R-NP-GFP and OVA is not simply due to general effects of PSI on antigen processing or K^b availability or export. Normalization of the data reveals that the relative rates of production of complexes from NP-GFP and KEKE-NP-GFP are highly similar, reaching a rate of complex formation half of that observed in untreated cells (Figure 3E). This suggests that these peptides derive nearly equally from rapidly and slowly degraded substrate pools at this time postinfection.

Time Required for Peptide Generation and Trafficking

We further examined the kinetics of antigen processing using the rVV-expressing MSIINFEKL. Although it is not technically feasible to measure the translation rate of this peptide, it is under the control of the same VV promoter as the other inserted genes, and its rate of translation should be similar. The peak rate of complex formation from MSIINFEKL is ~5-fold higher than that of R-NP-GFP. Thus, even the near complete degradation of R-NP-GFP does not come close to producing saturating amounts of peptide.

Complex formation from MSIINFEKL ceases 30 min after the addition of PSI (Figure 3F). Since peptides are degraded rapidly unless protected by MHC class I molecules (Malarkannan et al., 1995; Reits et al., 2003), association must occur within a few minutes of their synthesis. Consequently, virtually all complexes exit the endoplasmic reticulum (ER) and transit the secretory pathway within 30 min of their formation. Notably, the PSI-induced cessation of complex formation from R-NP-GFP (and OVA) demonstrated a 20 min lag relative to MSIINFEKL. This is consistent with the 10 min half-life of R-NP-GFP and suggests that OVA DRiPs are degraded with similar kinetics.

Quantitating Antigen Processing in Professional Antigen-Presenting Cells

We next studied the efficiency of antigen processing in VV-infected professional antigen-presenting cells (pAPC): bone marrow dendritic cells (BMDCs), the DC-like cell line DC2.4 (Shen et al., 1997), and macrophages (Mϕ). $CD11c^+$ BMDCs and DC2.4 cells expressed NP-GFP with similar kinetics and at similar levels as L-K^b cells, while $CD11b^+$ macrophages present in peritoneal exudates expressed NP-GFP at ~45% of the levels achieved in L-K^b and DCs (Figure 3G; data for L-K^b cells are replotted from Figure 1 for purposes of comparison). Notably, the generation of K^b-SIINFEKL complexes from NP-GFP now demonstrated nearly linear kinetics (Figure 3H) strongly suggesting that peptides derive principally from DRiPs. The efficiency of generating K^b-SIINFEKL complexes from NP-GFP, R-NP-GFP (Figure 3I), KEKE-NP-GFP (data not shown), and OVA (data not shown) by DCs and Mϕs was similar to L-K^b cells, as determined by calculating the ratio of cell surface complexes generated per quantity of protein substrate biosynthesized.

Discussion

Macroeconomics of Protein Synthesis and Degradation

We have measured rates of protein synthesis and degradation and the numbers of ribosomes and proteasomes in a model-cultured cell (Table 2). Although several of

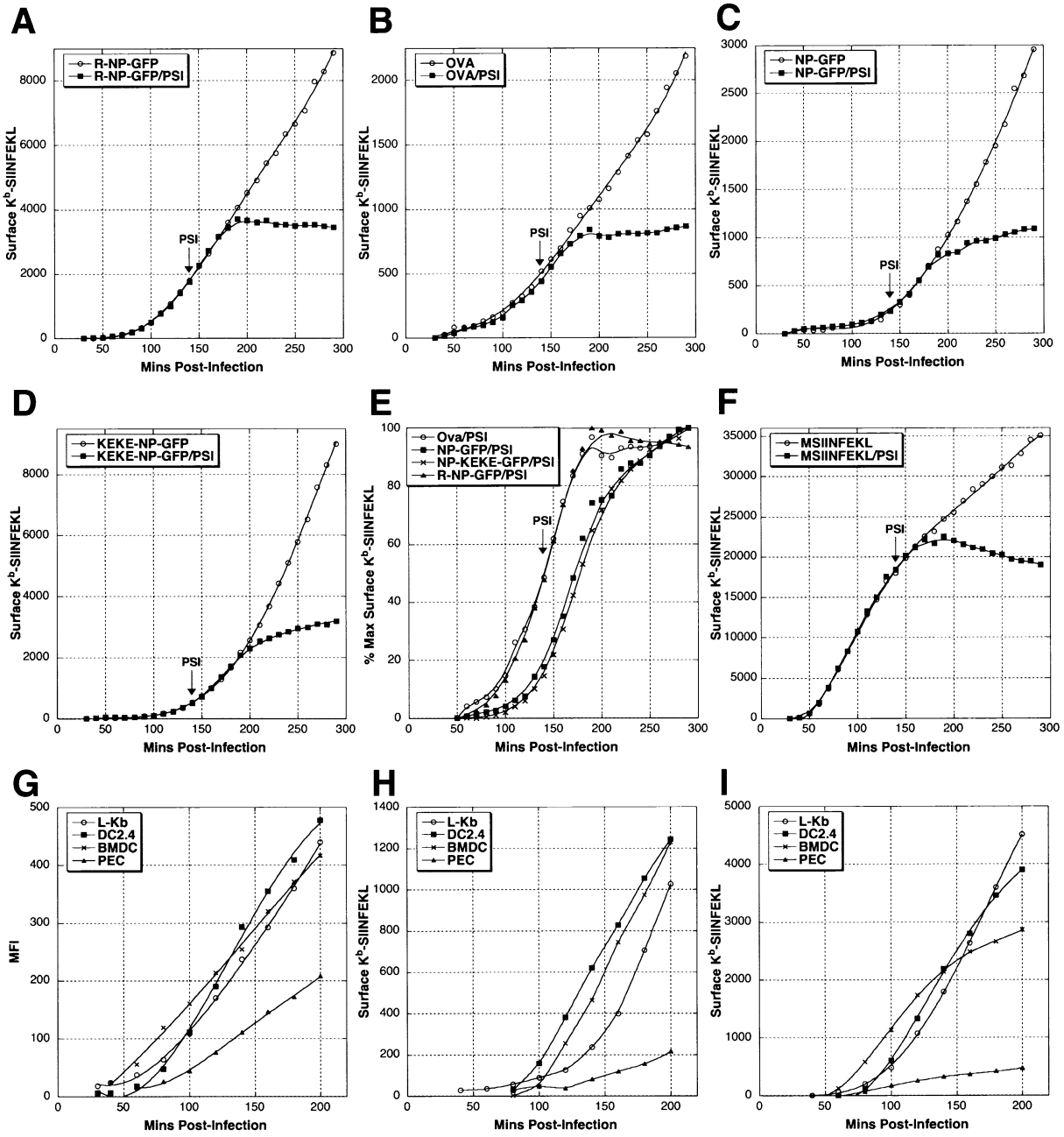

Figure 3. Generation of Surface K^b-SIINFEKL Complexes on rVV-Infected Cells

(A–D and F) Surface K^b-SIINFEKL levels on L-K^b cells infected with rVVs expressing OVA (A), R-NP-GFP (B), NP-GFP (C), KEKE-NP-GFP (D), or MSIINFEKL (F) and treated 140 min p.i. with protein synthesis inhibitors (squares) or left untreated (circles).

(E) Surface K^b-SIINFEKL levels on cells expressing OVA (circles), NP-GFP (squares), KEKE-NP-GFP (X), and R-NP-GFP (triangles) following treatment with protein synthesis inhibitors 140 min p.i. Surface K^b-SIINFEKL levels are expressed as the percent of maximum 25-D1.16 staining for each construct.

(G–I) DC-like DC2.4 cells (squares), bone marrow-derived dendritic cells (BMDC) (X), and peritoneal exudate macrophages (PEC) (triangles) were infected with rVV-expressing NP-GFP (G and H) or R-NP-GFP (I). GFP levels (G) and K^b-SIINFEKL complexes (H and I) were quantitated as described for L-K^b cells. GFP and surface K^b-SIINFEKL levels for L-K^b cells (circles) are replotted from Figures 1 and 2 for the purpose of comparison.

these values have been published before, it has always been in a piecemeal manner (separate laboratories working with different cells) that prevents integrating the data in anything but a theoretical manner (Yewdell, 2001). Remarkably, the theoretical values correlate reasonably well with the actual values we have determined. These values have some interesting implications.

Using textbook values relating the rRNA:tRNA or cellular protein:tRNA ratios (Alberts et al., 1994), we can calculate that L-K^b cells possess ~10–25 copies of tRNA

Table 2. The Protein Economy of L-K^b Cells

Production	
Proteins per cell	2.6×10^9
Ribosomes per cell	6×10^6
Translation rate	4×10^6 min^{-1}
% Required for cell division (24 hr)	43%
% Secreted or released	12%
% Ribosomes engaged in translation	>95%
tRNA per ribosome	10–25
% Cellular metabolism devoted to protein synthesis	45%
Destruction	
Proteasomes per cell	8×10^5
Overall degradation rate	1.8×10^6 min^{-1}
Newly synthesized proteins	1.3×10^6 min^{-1}
Long-lived proteins	5×10^5 min^{-1}
Proteasome activity	2.5 substrates degraded min^{-1}
Creative destruction	
Efficiency of SIINFEKL-K^b complex production	1/440–1/3000 substrates degraded per complex created

per ribosome. Since a complete set of tRNA comprises 32 species whose abundance differs by 10-fold, it means that the lower abundance tRNAs may be present at a ratio of 1 copy for every 20 ribosomes. The low ratio of tRNA to ribosomes makes it easy to understand how codon usage governs translation rates (Sharp and Li, 1986; Liljenstrom and von Heijne, 1987). If ribosomes translate proteins in compartments that limit access to tRNA, as evidence suggests (Stapulionis and Deutscher, 1995), then such compartments must contain multiple ribosomes. We can estimate that there must be ~20 ribosomes per compartment for each compartment to contain at least one of each tRNA species.

We find that L-K^b cells possess approximately eight times as many functional ribosomes as proteasomes. This precludes the pairing of a proteasome with each ribosome to create a translation/degradation complex. To the extent that proteins are truly degraded cotranslationally (Turner and Varshavsky, 2000), this means that proteasomes must be recruited to ribosomes. Given the density of ribosomes in the cytosol, the inter-proteasome-ribosome distance should never be much greater than the diameter of ribosomes, and given the velocity of proteasome diffusion in the cytosol (Reits et al., 1997), the time will be very short relative to the speed of translation.

Dividing the number of substrates degraded min^{-1} (2×10^6) by the number of functional proteasomes (8×10^5) reveals that each proteasome degrades an average of ~2.5 substrates min^{-1}. Taking the average size of a peptide generated by the proteasome as 7–8 residues (Kisselev et al., 1999) and the average size of a protein as 466 amino acids, the proteasome must be capable of cleaving at least 150 peptide bonds min^{-1}. This represents a minimal estimate of the turnover rate, since proteasomes (whose levels can only be increased relatively slowly due to their slow assembly times), must have residual capacity for degrading proteins when cells are damaged by chemical or physical stress.

Similar to other cells (Schubert et al., 2000), 25% of proteins synthesized by L-K^b cells appear to represent DRiPs. Since protein synthesis accounts for 45% of ATP utilization, this means that DRiP production consumes 11% of cellular energy and whatever additional energy costs (probably minor in comparison) are incurred during DRiP destruction. Protein synthesis is believed to consume between ~20% of the energy generated by adult mammals and a higher fraction in growing juveniles (Rolfe and Brown, 1997). A 25%–30% DRiP rate translates into wasting >6% of food consumption due to inefficient protein biosynthesis. On top of this must be added the energy devoted to creating the infrastructure for synthesizing (ribosomes, chaperones, tRNA, etc.) and destroying (proteasomes, Ub, etc.) DRiPs.

Could this be? As discussed previously (Yewdell et al., 2001), the true DRiP rate in vivo may be considerably lower than we measure in vitro. We must entertain the possibility, however, that high DRiP rates are a general feature of cells. Protein biosynthesis may simply be a difficult task, and investments in increasing efficiency may not be worth the cost. Alternatively (and risking heresy), perhaps we overvalue efficiency in biological systems. Only ~2% of the human genome encodes proteins. Though some noncoding DNA must be essential, retro transposons seem to be a clear-cut case of inefficiency. Rube Goldberg would be proud of mitochondria, which maintain a complete translation system and genome to produce just 13 proteins. Ultimately, selection pressure in evolution is exerted by other similarly inefficient organisms and not arbitrary standards of efficiency conjured by human intelligence.

Microeconomics of MHC Peptide Ligand Generation

Obtaining a valid estimate of the efficiency of generating class I ligands from protein substrates requires accurate knowledge of the numbers of complexes formed and substrates degraded. Obtaining the latter number is not a simple task for proteins traditionally thought of as metabolically stable, due to the uncertain proportion of nascent protein diverted to the DRiP pool. Montoya and del Val (1999) estimated the efficiency of generating an antigenic peptide from VV-encoded β-galactosidase but limited their analysis to the amount of protein synthesized as determined by enzymatic activity compared to purified β-galactosidase. They did not attempt to determine the DRiP fraction of β-galactosidase, leaving open

Table 3. Processing Efficiency and DRiP Rate

Experiment	Cell Type	Protein Molecules Degraded per Surface K^b-SIINFEKL Complex	DRiP Rate
1	L-K^b	1638	18.7%
2	L-K^b	1214	25.4%
3	L-K^b	994	31.5%
4	L-K^b	2292	20.9%
5	L-K^b	2031	27.8%
6	L-K^b	1772	29.0%
7	L-K^b	3122	37.4%
8	L-K^b	2872	30.9%
9	L-K^b	2026	22.6%
Avg		1995	27.1%
1	DC2.4	1780	44.8%
2	DC2.4	1226	23.0%
3	DC2.4	1211	25.7%
Avg		1406	31.2%
1	BMDC	1464	40.4%
2	BMDC	4400	55.8%
Avg		2932	48.1%
1	PEC	6481	42.6%
2	PEC	2960	22.0%
Avg		4720	32.3%

the question of the efficiency of peptide generation per substrate.

Determining the true DRiP fraction for any given protein poses technical hurdles (Yewdell et al., 2001). This is much less of a problem, however, for R-NP-GFP, which in being nearly completely degraded within minutes of its synthesis exhibits a DRiP rate of nearly 100%. Since NP-GFP, R-NP-GFP, and KEKE-NP-GFP are synthesized at comparable rates, we can use NP-GFP as a reference protein to calculate the rate of R-NP-GFP synthesis. Although an uncertain amount of newly synthesized NP-GFP is diverted to DRiPs, this can be accounted for by calculating the difference in the rate of K^b-SIINFEKL complex formation from the two proteins and dividing this by the difference in the rates of synthesis of stable proteins, which is essentially equal to the apparent rate of NP-GFP synthesis. By taking these rates shortly after the rate of production of complexes from R-NP-GFP peaks, we can minimize the contribution of peptides from the slowly degraded cellular NP-GFP pool.

Examination of Figure 3 shows that between 160 and 180 min postinfection, 970 complexes are generated from R-NP-GFP by L-K^b cells. Over the same period, 306 complexes were generated from NP-GFP. The corresponding increase in stable NP-GFP protein, which must be taken 50 min earlier (110–130 min postinfection) to allow for processing and transport of peptide-class I complexes, was 6.6×10^5 molecules synthesized. Thus, 6.6×10^5 more R-NP-GFP molecules were degraded than NP-GFP over this time period to generate an additional 664 K^b-SIINFEKL complexes. We can therefore calculate the efficiency of complex generation:

$$\frac{970 - 306}{6.6 \times 10^5} = 1/994. \quad (1)$$

Over nine independent experiments this number was relatively constant, ranging between 1/994 and 1/3122 (Table 3), with an average efficiency of 1 complex generated per 1995 R-NP-GFP molecules degraded. The efficiency of peptide generation was similar in pAPCs (Table 3), averaging 1 per 1406 substrates degraded by DC2.4 cells, 1 per 2932 substrates degraded by BMDC and 1 per 4720 substrates degraded by Mϕs.

The findings with VV-MSIINFEKL in L-K^b cells help explain this low efficiency. The much higher levels of K^b-SIINFEKL complex formation observed using this rVV demonstrates that TAP or MHC class I molecules are not limiting in the processing of NP-GFP constructs. The maximal rate of complex formation from MSIINFEKL (200 complexes min^{-1}) was achieved by 50 to 60 min postinfection. Given the 30 min delay for complex appearance at the cell surface, this means that peptide achieves near saturating levels between 20 and 30 min postinfection. At this time, MSIINFEKL peptide is expressed at a rate of ~10,000 molecules min^{-1} based on comparison to NP-GFP synthetic rates. Therefore, the observed ~200 complexes min^{-1} are created with an efficiency of ~2%.

Since 1 of every 50 peptides synthesized survives to form a stable surface K^b-SIINFEKL complex whereas complexes are generated from protein with an efficiency of 1 in 2000, this suggests the rate of suitable peptide production from protein is ~1 in 40. Cascio et al. (2001) reported that the efficiency of producing SIINFEKL or N-extended forms that can be further trimmed (cells are rich in amino exopeptidase activity against oligopeptides but lack carboxypeptidase activity) from OVA by incubation with standard or immunoproteasomes is approximately 1/16.

Given some wiggle room then, we can account for the efficiency of SIINFEKL production—proteasomes produce appropriate precursor peptides ~2.5% of the time, and only ~2% of these will survive the perils of the cytosol and voyage into the ER to find class I molecules, a net efficiency of .05% or 1/2000. Although the comparative data set is limited, SIINFEKL is produced

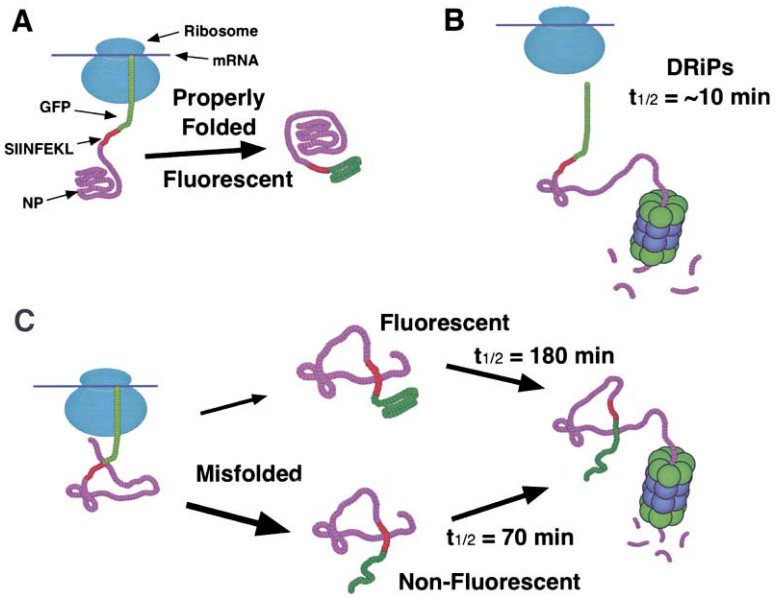

Figure 4. Possible Fates of Newly Synthesized Protein Molecules

(A) Properly folded nascent protein molecule. Stable, with long $t_{1/2}$. Protein is fluorescent due to properly folded GFP moiety. Represented by non-DRiP fraction of NP construct.

(B) Defective ribosomal product. Highly unstable, with $t_{1/2}$ = 10 min. Targeted for rapid degradation by the proteasome. Virtually all R-NP behaves as a DRiP, as well as a fraction of newly synthesized NP and KEKE-NP molecules.

(C) Improperly folded nascent protein molecule. Protein fails to fold to native conformation. GFP moiety may or may not fold properly, resulting in fluorescent and nonfluorescent protein populations. Unstable, with $t_{1/2}$ = 70–180 min. Predominant fate of non-DRiP fraction of KEKE-NP.

more efficiently than other defined determinants expressed under similar circumstances (Antón et al., 1997, 1998; Montoya and del Val, 1999). This is consistent with previous calculations, indicating that the overall efficiency of peptide generation from degraded molecules is on the order of 1/10,000 (Yewdell, 2001).

This is a far cry from previous determinations of the efficiency of proteasome-mediated peptide generation from bacterial proteins secreted into the cytosol of infected J774 cells (a Mϕ-like reticulum cell sarcoma), which was determined to be as high as one class I peptide complex generated for every three *L. monocytogenes* p60 proteins degraded (Villanueva et al., 1994; Sijts et al., 1996). What could account for this discrepancy? Probably real differences in processing efficiency combined with experimental errors. It is unlikely that macrophages are generally more adept at processing endogenous antigens, since we find that peritoneal Mϕs are actually less efficient than L-K^b cells and DCs in generating K^b-SIINFEKL complexes from R-NP-GFP. It is possible, however, that Mϕs possess specialized machinery that enables high efficiency processing of bacteria and other phagocytosed antigens. It was recently reported that phagosomes fuse with portions of the ER in Mϕs (Gagnon et al., 2002). Since proteasomes appear to participate in the processing of p60 (Zwickey and Potter, 1999), any gains in processing efficiency would have to entail export of bacterial peptides to the cytosol from the ER-phagosome and their reimportation into the ER-phagosome or ER.

Fully acknowledging the seminal importance of the quantitative studies by Pamer and colleagues, we note that they may have overestimated the number of peptides produced and underestimated the amount of protein degraded. Differences between naturally processed peptides and their synthetic counterparts will lead to an overestimation of the number of peptides generated by cells if, as is often the case, T_{CD8+} preferentially recognize the naturally processed versions. Side chain modification can often only be detected by mass spectroscopic analysis, which was not used to demonstrate the identity of synthetic and natural *Listeria*-derived peptides. The amount of p60 introduced into the cytosol was not determined directly but was based on the rate of secretion of p60 by extracellular bacteria. This was measured using antibodies that may not recognize all forms of secreted p60. Notably, the $t_{1/2}$ of p60 in J774 cells measured using these antibodies was 90 min while peptide loading of class I molecules was virtually complete within 30 min of addition of a bacterial protein synthesis inhibitor. This suggests a discrepancy between the antibody reactive-p60 and p60 that provides antigenic peptides.

Although the efficiency of peptide generation from endogenous viral proteins appears to be relatively low, it may still be sufficient to serve the purposes of the immune system. A key feature of many viral infections is the nearly complete replacement of host mRNA translation with viral mRNA. Since T_{CD8+} require only tens to hundreds of class I peptide complexes for activation, this, in combination with a high DRiP rate, should enable T_{CD8+} recognition of infected cells in a time frame that enables lysis of infected cells prior to completion of the infectious cycle.

Biosynthesized Proteins as Sources of Peptide

Khan et al. (2001) reported that generation of an antigenic peptide from a protein requires continued production of mRNA encoding the protein, as shown over the course of hours after blocking transcription. We show that the kinetics of K^b-SIINFEKL complex generation from OVA (its natural protein source) under normal conditions and after blocking protein synthesis behaves exactly as predicted for a short-lived DRiP. This provides conclusive evidence for the validity of the DRiP hypothesis for the generation of peptides from a specific, genetically unmodified gene product.

Unlike OVA, SIINFEKL production from NP-GFP continues at a reduced rate after blocking protein synthesis. Over the same interval, GFP levels remain virtually constant when measured with an extremely high degree

of precision in individual cells by flow cytometry. We interpret this to mean that peptides derive from a nonfluorescent subpopulation of NP-GFP that is degraded relatively slowly. This interpretation is fully consistent with the acceleration of peptide production as the infection period proceeds. In this manner NP-GFP behaves like KEKE-NP-GFP, which provides a model for a slowly degraded substrate. (Figure 4 illustrates the possible conformational states and fates of the chimeric NP proteins we utilized.) Even KEKE-NP-GFP demonstrates two forms, since its biochemical decay is significantly faster than its decay in fluorescence when protein synthesis is halted. The nonfluorescent form of NP-GFP may never have been properly folded, in which case it can be considered a slowly degraded DRiP. The absolute stability of NP-GFP fluorescence in the presence of PSI suggests that this is the case, but we cannot rule out the possibility that peptides derive from a pool of native NP-GFP that unfolded well after translation.

If class I peptide complexes are produced with similar efficiency from rapidly degraded NP-GFP DRiPs and R-NP-GFP, we can calculate the percentage of nascent NP-GFP that is diverted to this pool. To limit the contribution of the more slowly degraded cellular substrate pool, we use the number of complexes generated between 110 and 130 min postinfection with NP-GFP:

$$(306 \text{ complexes}) \times (994 \text{ substrates/complex}) = 3.04 \times 10^5 \text{ substrates.} \quad (2)$$

Dividing the number of rapidly degraded proteins by the total number of NP-GFP molecules synthesized gives us the DRiP rate:

$$\frac{(3.04 \times 10^5 \text{ substrates})}{(6.6 \times 10^5 \text{ NP}) + (3.04 \times 10^5 \text{ DRiPs})} = 31.5\%. \quad (3)$$

As seen in Table 3, this ranged from 19% to 37% over nine experiments for L-K^b cells, with an average value of 27%—remarkably similar to the overall DRiP rate of 25%. Similar calculations for pAPCs reveal a comparable range of DRiP rates.

As can be seen in Figure 2A, the rate of K^b-SIINFEKL production from KEKE-NP-GFP accelerates as the size of the cellular KEKE-NP-GFP pool increases, eventually overtaking the rate of production from R-NP-GFP. This is only possible if K^b-SIINFEKL complexes are generated from the cellular KEKE-NP-GFP pool more efficiently than from the short-lived DRiPs.

The efficiency of K^b-SIINFEKL generation from the long-lived KEKE-NP-GFP pool can be calculated by taking advantage of the fact that the rates of KEKE-NP-GFP synthesis and degradation approach equilibrium by 5 hr postinfection. At this time the rate of synthesis is 3.2×10^6 molecules hr^{-1}. If 31.5% of these molecules (1×10^6 hr^{-1}) are short-lived DRiPs, then the net synthetic rate is 2.2×10^6 hr^{-1}, which equals the degradation rate. The rate of K^b-SIINFEKL production at this time is 6×10^3 complexes hr^{-1}. Of these, we calculate that 1×10^3 are generated from the short-lived DRiP fraction (1×10^6 DRiPs degraded with an efficiency of 1 complex per 994 substrates). The remaining 5×10^3 complexes should be derived from the 2.2×10^6 molecules of KEKE-NP-GFP degraded hr^{-1} from the long-lived pool. This yields a calculated efficiency of 1 K^b-SIINFEKL complex generated per 440 KEKE-NP-GFP molecules degraded.

If this efficiency applies to the pool of nonfluorescent NP-GFP discussed above, we can calculate that the 447 complexes generated from the slowly degraded pool in the last hour of infection (1365 total complexes minus the 918 complexes from rapidly degraded DRiPs using the initial rate) would represent the degradation of 2.0×10^5 substrates, which represents ~2.5% of the total NP pool at this time.

We can use these values to bolster our conclusion that after blocking protein synthesis complexes are generated from nonfluorescent NP-GFP. Over the last 100 min of the infection in the presence of protein synthesis inhibitors (when GFP levels are stable), 300 complexes were generated, which would represent degradation of $300 \times 440 = 1.3 \times 10^5$ substrates. If these molecules were fluorescent, this would represent 13 fluorescent units, which is well within the precision of our measurements.

The more efficient generation of class I peptide complexes from KEKE-NP-GFP than from R-NP-GFP suggests that proteasomes display heterogeneity in their capacity to generate class I peptide ligands. Little is known about functional differences between proteasomes—given their abundance and involvement in myriad cellular processes it is likely that proteasomes display considerable heterogeneity in function, in addition to those attributed to the alterations associated with immunoproteasomes.

Experimental Procedures

Cells and Viruses

L-K^b and DC2.4 cells were provided, respectively, by Sheil (West Virginia University, Morgantown, WV) and Rock (University of Massachusetts Medical School, Worcester, MA). Mϕs elicited from C57BL/6 mice by intraperitoneal injection of 1 ml 3% (w/v) thioglycollate solution were harvested 5–6 days postinjection and used immediately. BMDC obtained from femurs were propagated in media supplemented with 20% FBS and 10% supernatant from X63 cells transfected with murine GM-CSF. Nonadherent cells were removed on days 2 and 4. Adherent cells were used for assays on days 6–7 after harvest.

rVVs expressing SIINFEKL-containing proteins have been described (Antón et al., 1999). NP-GFP fusion proteins contain SIINFEKL peptide at the C terminus of NP followed by ARDPPVAT followed by EGFP. Cells were infected at a multiplicity of infection (MOI) of 10 for 15 min at 37°C with constant agitation in balanced salt solution containing 0.1% bovine serum albumin (BSS/BSA). Cells were then incubated at 37°C in growth media for the remainder of the assay in the presence of 25 μg/ml cytosine arabinoside. Protein synthesis was inhibited by the addition of cycloheximide and emetine (Sigma, St. Louis, MO) to a final concentration of 25 μg /ml each.

Immunoblotting

L-K^b cells (5×10^5) were lysed in 1 ml 95°C SDS-PAGE sample buffer and boiled for 10 min. Serial 2-fold dilutions were made into sample buffer containing uninfected L-K^b cell lysates (5×10^5 cells/ml) to maintain a constant protein concentration in samples. Samples were separated in 10%–12.5% SDS-PAGE gels and transferred to PVDF membranes. Immunoblots were incubated with rabbit antibodies raised to a synthetic peptide corresponding to NP$_{2\text{-}13}$. Proteasome immunoblots were probed with a mouse mAb that binds the p29K α-subunit (ICN Biomedicals, Costa Mesa, CA). Ribosome immunoblots were probed with human anti-ribosomal P autoimmune serum (Immunovision, Springdale, AK). Blots were developed with horseradish peroxidase-coupled antibodies using a chemilumines-

cent peroxide substrate. Luminescence was recorded on Biomax MR film (Eastman Kodak, Rochester, NY), digitized, and analyzed using ImageQuant software (Molecular Dynamics Inc., Sunnyvale, CA). Standard curves were used to determine concentrations of corresponding proteins in samples containing lysates from rVV-infected L-K^b cells.

NP-GFP standards were prepared by determining the total protein concentration in purified preparations of influenza virus A/Puerto Rico/8/34. The percentage NP-GFP of total viral protein was determined by SDS-PAGE. Purified proteasomes and ribosomes were the kind gifts, respectively, of DeMartino (University of Texas Southwestern Medical Center, Dallas, TX) and Nicchitta (Duke University Medical Center, Durham, NC).

Cytofluorography

K^b-SIINFEKL levels were determined by incubating cells for 30 min on ice with the 25-D1.16 antibody (Porgador et al., 1997) conjugated to Alexa Fluor 647 (Molecular Probes, Eugene, OR). Cellular GFP and Alexa Fluor 647 levels were determined on a FACScalibur cytofluorograph (Beckton Dickinson, San Jose, CA) using CellQuest (Beckton Dickinson) software, and data were analyzed using FlowJo (Tree Star, San Carlos, CA) software.

Purified 25-D1.16 mAb was conjugated to either fluorescein isothiocyanate (FITC) (Roche) or Alexa Fluor 647, and fluorescence to protein ratios (F:P) for each conjugate were determined. Antibody preparations were titrated against SIINFEKL peptide L-K^b cells to ensure that all staining was performed with saturating concentrations of Ab. To quantitate surface K^b-SIINFEKL levels, L-K^b cells were incubated with 2-fold dilutions of SIINFEKL peptide and stained with 25-D1.16 conjugated to either FITC or Alexa Fluor 647, and fluorescence levels were determined by cytofluorography. Fluorescence levels for FITC-coated calibration beads (DAKO) were determined in parallel and used to construct a standard curve of FITC molecules versus mean fluorescence intensity (MFI). The F:P for FITC-conjugated 25-D1.16 was then used to calculate the number of antibody molecules bound per cell. Calibration standards for Alexa Fluor 647 are not commercially available; therefore, the ratio of MFI to bound antibody for Alexa Fluor 647-conjugated 25-D1.16 was determined by direct comparison with FITC-25-D1.16-stained L-K^b cells.

Peritoneal macrophages, BMDC, and DC2.4 were incubated with 2.4G2 culture supernatant for 20 min on ice to block Fc-receptor-mediated binding prior to staining with 25-D1.16.

Pulse Labeling of Cellular Proteins

L-K^b cells were labeled at 37°C for 10 min with 100 μCi [^{3}H]-Leu (153 Ci/mM) (Amersham) in 180 μl of I^+ (which contains 0.802 mM Leu). Labeling was stopped by adding ice-cold media containing excess (10 mM) Leu, and cell pellets were washed once in this same medium. Cell pellets were frozen on dry ice, thawed briefly, and lysed in SDS-PAGE sample buffer at 95°C. Cell lysates were transferred onto filter paper, and protein was precipitated with 10% TCA and then washed extensively with 70% ethanol. Radioactivity was measured by scintillation counting. Labeling of L-K^b cells with [^{35}S]-Met (Amersham) was performed as described for [^{3}H]-Leu. Cell lysates were separated in 10% SDS-polyacrylamide gels. Gels were dried and then scanned on a Typhoon 8600 imager, and digitized images were analyzed using ImageQuant software. To measure secretion of newly synthesized proteins from L-K^b cells, [^{35}S]-Met labeled cells were chased for up to 2 hr containing nonradiolabeled Met. Cell pellets and supernatants from each time point were collected, lysed, and transferred to filter paper and quantitated by scintillation counting as described above.

In preliminary experiments we established that incorporation of [^{3}H]-Leu into proteins with time was absolutely linear under these conditions with no detectable lag following incubation for as short as 1 min. For reasons we do not understand fully, labeling of proteins with [^{35}S]-Met resulted in ~1/10 of the specific activity obtained with [^{3}H]-Leu, which precluded the use of [^{35}S]-Met for absolute determination of protein synthesis rates. Due to the low sensitivity of detecting [^{3}H]-Leu with PhosphorImager screens, we used [^{35}S]-Met to determine the fraction of total protein allotted to NP synthesis.

ATP Consumption

The proportion of cellular energy devoted to protein synthesis in L-K^b cells was determined by measuring O_2 consumption in the presence or absence of protein synthesis inhibitors as previously described (Buttgereit et al., 1992).

Acknowledgments

We thank Sandy Hayes, Felicita Hornung, and David Tscharke for critical reading of the manuscript and insightful comments.

Received: January 13, 2003
Revised: January 13, 2003

References

Alberts, B., Bray, D., Lewis, J., Raff, M., Roberts, K., and Watson, J.D. (1994). Molecular Biology of the Cell (New York: Garland Publishing).

Antón, L.C., Yewdell, J.W., and Bennink, J.R. (1997). MHC class I-associated peptides produced from endogenous gene products with vastly different efficiencies. J. Immunol. *158*, 2535–2542.

Antón, L.C., Snyder, H.L., Bennink, J.R., Vinitsky, A., Orlowski, M., Porgador, A., and Yewdell, J.W. (1998). Dissociation of proteasomal degradation of biosynthesized viral proteins from generation of MHC class I-associated antigenic peptides. J. Immunol. *160*, 4859–4868.

Antón, L.C., Schubert, U., Bacik, I., Princiotta, M.F., Wearsch, P.A., Gibbs, J., Day, P.M., Realini, C., Rechsteiner, M.C., Bennink, J.R., and Yewdell, J.W. (1999). Intracellular localization of proteasomal degradation of a viral antigen. J. Cell Biol. *146*, 113–124.

Buttgereit, F., Brand, M.D., and Muller, M. (1992). ConA induced changes in energy metabolism of rat thymocytes. Biosci. Rep. *12*, 109–114.

Cascio, P., Hilton, C., Kisselev, A.F., Rock, K.L., and Goldberg, A.L. (2001). 26S proteasomes and immunoproteasomes produce mainly N-extended versions of an antigenic peptide. EMBO J. *20*, 2357–2366.

Gagnon, E., Duclos, S., Rondeau, C., Chevet, E., Cameron, P.H., Steele-Mortimer, O., Paiement, J., Bergeron, J.J., and Desjardins, M. (2002). Endoplasmic reticulum-mediated phagocytosis is a mechanism of entry into macrophages. Cell *110*, 119–131.

Heim, R., Cubitt, A.B., and Tsien, R.Y. (1995). Improved green fluorescence. Nature *373*, 663–664.

Hershko, A., and Ciechanover, A. (1998). The ubiquitin system. Annu. Rev. Biochem. *67*, 425–479.

Khan, S., de Giuli, R., Schmidtke, G., Bruns, M., Buchmeier, M., van Den, B.M., and Groettrup, M. (2001). Cutting edge: neosynthesis is required for the presentation of a T cell epitope from a long-lived viral protein. J. Immunol. *167*, 4801–4804.

Kisselev, A.F., Akopian, T.N., Woo, K.M., and Goldberg, A.L. (1999). The sizes of peptides generated from protein by mammalian 26 and 20 S proteasomes. Implications for understanding the degradative mechanism and antigen presentation. J. Biol. Chem. *274*, 3363–3371.

Liljenstrom, H., and von Heijne, G. (1987). Translation rate modification by preferential codon usage: intragenic position effects. J. Theor. Biol. *124*, 43–55.

Malarkannan, S., Goth, S., Buchholz, D.R., and Shastri, N. (1995). The role of MHC class I molecules in the generation of endogenous peptide/MHC complexes. J. Immunol. *154*, 585–598.

Montoya, M., and del Val, M. (1999). Intracellular rate-limiting steps in MHC class I antigen processing. J. Immunol. *163*, 1914–1922.

Nandi, D., Woodward, E., Ginsburg, D.B., and Monaco, J.J. (1997). Intermediates in the formation of mouse 20S proteasomes: implications for the assembly of precursor beta subunits. EMBO J. *16*, 5363–5375.

Nissen-Meyer, J., and Eikhom, T.S. (1976). An excess of the small ribosomal subunits and a higher rate of turnover of the 60 S than of the 40 S ribosomal subunits in L cells grown in suspension culture. J. Mol. Biol. *101*, 211–221.

Palmiter, R.D. (1975). Quantitation of parameters that determine the rate of ovalbumin synthesis. Cell *4*, 189.

Porgador, A., Yewdell, J.W., Deng, Y., Bennink, J.R., and Germain, R.N. (1997). Localization, quantitation, and in situ detection of specfic peptide-MHC class I complexes using a monoclonal antibody. Immunity *6*, 715–726.

Reits, E.A.J., Benham, A.M., Plougastel, B., Neefjes, J., and Trowsdale, J. (1997). Dynamics of proteasome distribution in living cells. EMBO J. *16*, 6087–6094.

Reits, E.A., Vos, J.C., Gromme, M., and Neefjes, J. (2000). The major substrates for TAP in vivo are derived from newly synthesized proteins. Nature *404*, 774–778.

Reits, E., Griekspoor, A., Neijssen, J., Groothuis, T., Jalink, K., van Veelen, P., Janssen, H., Calafat, J., Drijfhout, J.W., and Neefjes, J. (2003). Peptide diffusion, protection, and degradation in nuclear and cytoplasmic compartments before antigen presentation by MHC class I. Immunity *18*, 97–108.

Rock, K.L., and Goldberg, A.L. (1999). Degradation of cell proteins and the generation of MHC class I-presented peptides. Annu. Rev. Immunol. *17*, 739–779.

Rock, K.L., York, I.A., Saric, T., and Goldberg, A.L. (2002). Protein degradation and the generation of MHC class I-presented peptides. Adv. Immunol. *80*, 1–70.

Rolfe, D.F., and Brown, G.C. (1997). Cellular energy utilization and molecular origin of standard metabolic rate in mammals. Physiol. Rev. *77*, 731–758.

Schubert, U., Anton, L.C., Gibbs, J., Norbury, C.C., Yewdell, J.W., and Bennink, J.R. (2000). Rapid degradation of a large fraction of newly synthesized proteins by proteasomes. Nature *404*, 770–774.

Sharp, P.M., and Li, W.H. (1986). An evolutionary perspective on synonymous codon usage in unicellular organisms. J. Mol. Evol. *24*, 28–38.

Shen, Z., Reznikoff, G., Dranoff, G., and Rock, K.L. (1997). Cloned dendritic cells can present exogenous antigens on both MHC class I and class II molecules. J. Immunol. *158*, 2723–2730.

Sijts, A.J., Neisig, A., Neefjes, J., and Pamer, E.G. (1996). Two *Listeria monocytogenes* epitopes are processed from the same antigen with different efficiencies. J. Immunol. *156*, 683–692.

Stapulionis, R., and Deutscher, M.P. (1995). A channeled tRNA cycle during mammalian protein synthesis. Proc. Natl. Acad. Sci. USA *92*, 7158–7161.

Turner, G.C., and Varshavsky, A. (2000). Detecting and measuring cotranslational protein degradation in vivo. Science *289*, 2117–2120.

Villanueva, M.S., Fischer, P., Feen, K., and Pamer, E.G. (1994). Efficiency of MHC class I antigen processing: a quantitative analysis. Immunity *1*, 479–489.

Wheatley, D.N. (1989). Protein turnover in relation to growth status and the cell cycle in cultured mammalian cells. Revis. Biol. Celular *21*, 377–400.

Yewdell, J.W. (2001). Not such a dismal science: the economics of protein synthesis, folding, degradation and antigen processing. Trends Cell Biol. *11*, 294–297.

Yewdell, J.W., Schubert, U., and Bennink, J.R. (2001). At the crossroads of cell biology and immunology: DRiPs and other sources of peptide ligands for MHC class I molecules. J. Cell Sci. *114*, 845–851.

Zwickey, H.L., and Potter, T.A. (1999). Antigen secreted from noncytosolic Listeria monocytogenes is processed by the classical MHC class I processing pathway. J. Immunol. *162*, 6341–6350.